(UPM). Figure 9 shows a picture of the reflectarray breadboard in the anechoic chamber.

The radiation patterns have been measured in elevation and azimuth planes for both polarizations. Figure 10 shows the radiation patterns measured at several frequencies for the H-polarization, which is the one that produces a higher cross-polarization, the patterns being very similar for the V-polarization, but with lower levels of cross-polarization. These results show stable radiation patterns in the measured frequency band (12.97–14.25 GHz).

A good agreement is observed between the simulated and measured radiation patterns for both copolar and cross-polar components, as shown in Figure 11 for H-polarization at 14 GHz. There are only slight discrepancies in the side lobes, which can be attributed to phase errors produced by tolerance errors in the thickness of the dielectric layers and in the dimensions of the patches. The experimental results confirm that a XPD better than 30 dB is achieved for both polarizations in the measured frequency band 12.97–14.25 GHz.

### 4. CONCLUSIONS

An offset reflectarray demonstrator has been designed, manufactured and tested to demonstrate that a significant reduction in the cross-polarization is achieved by exploiting the zero-crossing of the reflection coefficient for the cross-polarized field components. The comparison of the simulated results with the measurements shows good agreement in both copolar and cross-polar components. A reduction better than 5 dB in the levels of cross-polarization for both polarizations is achieved, providing a cross-polar discrimination better than 30 dB in a wide frequency bandwidth, from 12.97 to 14.25 GHz, which is compliant with the very stringent requirements of dual-polarization Telecomm antennas in space applications.


### ACKNOWLEDGMENTS

This research was supported by the Ministry of Science and Technology, under the projects TEC2010-17-567 and Terasense, Consolider-Ingenio 2010.


### REFERENCES


1. C. Han, J. Huang, and K. Chang, A high efficiency offset-fed X/Ka dual-band reflectarray using thin membranes, IEEE Trans Antennas Propag 53 (2005), 2792–2798.
2. D.M. Pozar, S.D. Targonski, and R. Pokuls, A shaped-beam microstrip patch reflectarray, IEEE Trans Antennas Propag 47 (1999), 1167–1173.
3. J.A. Encinar and J.A. Zornoza, Three-layer printed reflectarrays for contoured beam space applications, IEEE Trans Antennas Propag 52 (2004), 1138–1148.
4. J.A. Encinar, L. She Datashvili, J.A. Zornoza, M. Arrebola, M. Sierra-Castaner, J.L. Besada-Sanmartin, H. Baier, and H. Legay, Dual-polarization dual-coverage reflectarray for space applications, IEEE Trans Antennas Propag 54 (2006), 2827–2837.
5. D.M. Pozar, Bandwidth of reflectarrays, Electron Lett 39 (2003), 1490–1491.
6. J. Huang, Bandwidth study of microstrip reflectarray and a novel phased reflectarray concept, In: IEEE International Symposium on Antennas and Propagation, Newport Beach, CA, June 18–23, 1995.
7. J.A. Encinar, Design of two-layer printed reflectarrays using patches of variable size, IEEE Trans Antennas Propag 49 (2001), 1403–1410.
8. J.A. Encinar and J.A. Zornoza, Broadband design of three-layer printed reflectarrays, IEEE Trans Antennas Propag 51 (2003), 1662–1664.
9. N. Misran, R. Cahill, and V. Fusco, Design optimisation of ring elements for broadband reflectarray antennas, IEE Proc Microwaves Antennas Propag 150 (2003), 440–444.
10. E. Carrasco, J.A. Encinar, and M. Barba, Bandwidth improvement in large reflectarrays by using true-time delay, IEEE Trans Antennas Propag 56 (2008), 2496–2503.
11. M. Bozzi, S. Germani, and L. Perregrini, Performance comparison of different element shapes used in printed reflectarrays, IEEE Antennas Wireless Propag Lett 2 (2003), 219–222.
12. J.A. Encinar, M. Arrebola, L.F. de la Fuente, and G. Toso, A transmit-receive reflectarray antenna for direct broadcast satellite applications, IEEE Trans Antennas Propag 59 (2011), 3255–3264.
13. J.A. Encinar, Reduction of cross-polarization in contoured beam reflectarrays using a three-layer configuration, In: Antennas and Propagation International Symposium, 2007 IEEE, 9–15 June, 2007, pp. 5303–5306.
14. C. Wan and J.A. Encinar, Efficient computation of generalized scattering matrix for analyzing multilayered periodic structures, IEEE Trans Antennas Propag 43 (1995), 1233–1242.
15. K. Pontoppidan, Technical Description of GRASP8 (TICRA).




# PHOTON-PAIR STATES AND VIOLATION OF CHSH INEQUALITY


**Luís P. Martins,[1,2] Álvaro J. Almeida,[1,2] Paulo S. André,[1,2] and Armando N. Pinto[2,3]**

[1] Department of Physics, University of Aveiro, Campus Universitário de Santiago, 3810-193 Aveiro, Portugal; Corresponding author: luismppmartins@hotmail.com

[2] Instituto de Telecomunicações, Campus Universitário de Santiago, 3810-193 Aveiro, Portugal

[3] Department of Electronics, Telecommunications and Informatics, University of Aveiro, Campus Universitário de Santiago, 3810-193 Aveiro, Portugal



*Received 20 January 2012*



**ABSTRACT:** *In addition to Bell's original inequality, John Clauser, Michael Horne, Abner Shimony, and Richard Holt (CHSH) developed a special form of Bell's inequality which gives classical limits to the expected correlation between two particles. We present a theoretical demonstration of the maximum value for violation of CHSH inequality,* $S = 2\sqrt{2}$*, for the pure entangled quantum state. Using the spontaneous four-wave mixing process, we generate polarization-entangled photon pairs in a highly nonlinear fiber (HNLF) loop, for experimental verification. Using a nonentangled quantum state, we show theoretically that the violation of CHSH inequality is only a property of entangled states. We also show the theoretical solution of violation of the CHSH inequality for a general Greenberger–Horne–Zeilinger state and for an arbitrary state of two particles.* © 2012 Wiley Periodicals, Inc. Microwave Opt Technol Lett 54:2454–2461, 2012; View this article online at wileyonlinelibrary.com. DOI 10.1002/mop.27127



**Key words:** *CHSH inequality; locality; quantum entanglement; four-wave mixing; highly nonlinear fiber*


### 1. INTRODUCTION

Quantum cryptography allows the exchange of information in a perfectly secure way. There are several quantum protocols, as BB84 [1] or E91 [2], that can be implemented in quantum communications using single and entangled photon pairs, respectively. There are several works that show that there is a direct link between the security of the quantum communication protocols and the violation of Bell inequalities [3]. The John Clauser, Michael Horne, Abner Shimony, and Richard Holt (CHSH) inequality [4] is a convenient way to express Bell's inequality. Bell showed that complete and local theories (i.e., the

measurements on one particle do not affect the measurements on the other) lead to different statistical results of standard quantum theory [5, 6]. This result is showed in the famous Bell inequality. The Bell inequality reflects the constraints on statistical correlations of measurements imposed by local theories of hidden variables (LTHVs), and it is incompatible with reality as it was already verified experimentally [7–11], and with the quantum theory [5, 6]. For the pure states, the problem of violating the Bell type inequalities has been completely solved [12–15]. However, for mixture states, the problem is more difficult, even for the simplest case of two particles [16]. The Horodecki family presented an effective criterion for violating CHSH inequality for an arbitrary mixed quantum state of two particles [17].

There are many ways to generate entangled photon pairs. However, the four-wave mixing (FWM) is one of the most promising, because it generates the entangled photons inside the optical fiber [18]. The spontaneous FWM is a third-order optical nonlinear process, in which two pump photons are annihilated and a signal-idler photon pair is generated [19]. The generation of entangled photon pairs inside an optical fiber is very important to "quantum communication systems" over optical fiber networks [20, 21]. The violation of CHSH inequality can be used to check the generation of entangled states [22].

We use the FWM process (in the degenerate case, in which the optical frequencies of the two pump photons are the same) to generate polarization-entangled photon pairs in a highly nonlinear fiber (HNLF) loop, in order to experimentally verify the entanglement effect. We present an analytical proof for the maximum value allowed for violation of CHSH inequality, that is, $S = 2\sqrt{2}$, for the pure entangled quantum state. From the solution for the pure entangled quantum state we generalize the solution of the violation of the CHSH for general Greenberger–Horne–Zeilinger (GHZ) states and then for any arbitrary state of two particles, using the alternative method to Horodecki's method [17]. This general solution appears directly from the correlation function, and so it can be easily generalized to $N$ particles. We also show that the violation of CHSH inequality is a characteristic of entangled states only, that is, the nonentangled state do not violates the CHSH inequality, and for that, it can be described by LTHVs.

This article contains four sections. In Section 2, we present the derivation of Bell's inequality and find the theoretically solution for the violation of CHSH inequality for an entangled state, for the general GHZ state and for an arbitrary state. We also show the nonentangled quantum state case. In section III we present the experimental verification of quantum entanglement generation. The main conclusions of this article are presented in Section 4.

## 2. QUANTUM STATES AND CHSH INEQUALITY

The entangled states arise when more than one particle is in the same Hilbert space, that is, when it is not possible to factorize the state in individual states. These states are purely quantum, without an equivalent in classic theory. Mathematically, an entangled state between two particles can be written as

$$|\Psi_{\text{entanged}}\rangle = \sum_{i}^{\infty} |a_i\rangle_1 |b_i\rangle_2. \tag{1}$$

If we consider a system with two photons in two different states of polarization (horizontal and vertical),

$$|\Psi_{\text{entangled}}\rangle = \frac{1}{\sqrt{2}}\Big[|H\rangle_1|H\rangle_2 + |V\rangle_1|V\rangle_2\Big], \tag{2}$$

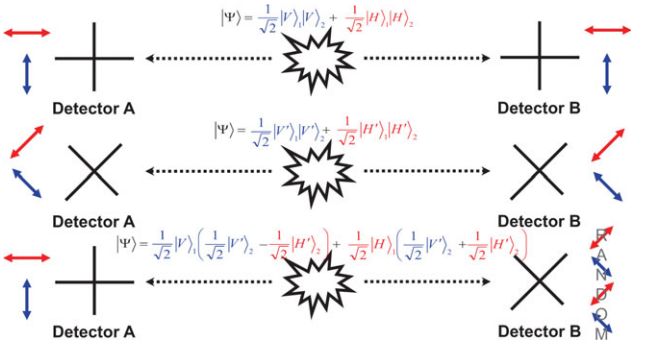


**Figure 1** Scheme of polarization measurement using two different basis. The states are written as a function of the basis of the measurement device. [Color figure can be viewed in the online issue, which is available at wileyonlinelibrary.com]

where this state is known as one of Bell states or the pure entangled quantum state. The two particles travel in opposite directions, where they will be detect by devices that measure their polarizations and that are rotated by $\alpha$ for particle 1 and by $\beta$ for particle 2, from the horizontal state. The state of the measurement device rotated by $\alpha$ is written according to,

$$|H\rangle_\alpha = \cos(\alpha)|H\rangle + \sin(\alpha)|V\rangle \tag{3}$$

and

$$|V\rangle_\alpha = -\sin(\alpha)|H\rangle + \cos(\alpha)|V\rangle. \tag{4}$$

The probabilities to obtain photons in a given polarization are,

$$\begin{aligned}
P_{V'_1,V'_2}(\alpha,\beta) &= |\langle V'|_\alpha \langle V'|_\beta \Psi\rangle|^2 = \frac{1}{2}\cos^2(\beta-\alpha);\\
P_{V'_1,H'_2}(\alpha,\beta) &= |\langle V'|_\alpha \langle H'|_\beta \Psi\rangle|^2 = \frac{1}{2}\sin^2(\beta-\alpha);\\
P_{H'_1,V'_2}(\alpha,\beta) &= |\langle H'|_\alpha \langle V'|_\beta \Psi\rangle|^2 = \frac{1}{2}\sin^2(\beta-\alpha);\\
P_{H'_1,H'_2}(\alpha,\beta) &= |\langle V'|_\alpha \langle V'|_\beta \Psi\rangle|^2 = \frac{1}{2}\cos^2(\beta-\alpha),
\end{aligned} \tag{5}$$

where $P_{V'_1,V'_2}(\alpha,\beta)$ represents the probability that both photons are vertically polarized and the measurement devices rotated by $\alpha$ and $\beta$, for photons 1 and 2, respectively, and analogously for another terms. We can see that only when $\beta - \alpha = 0$ exists perfect correlation, that is, we measure the same polarization in both devices. For all the other cases we have different levels of correlation, and only when $\beta - \alpha = 45°$ we can have a perfectly random behavior, that is, all polarizations are possible with the same probability. The scheme of Figure 1 illustrates this situation.

### 2.1. Bell Theory

To demonstrate Bell's inequality, we consider a system with two photons with the state described in Eq. (2). As mentioned above, the two particles travel in opposite directions, where they will be detected by devices that measure their polarizations and the devices are rotated by $\alpha$ for particle 1 and by $\beta$ for particle 2, in relation to the horizontal state. For hypothesis, the description of the states is given as a function of a set of indeterminate hidden variables that we call $\lambda$.

The measurements of the polarization of particles 1 and 2 are represented by letters $A$ and $B$, respectively. The measured

values are $+1$ (vertical polarization) or $-1$ (horizontal polarization), and $A$ and $B$ behave like random variables. Our notion of locality requires that $A$ only depends on $\lambda$ and $\alpha$, thus as $B$ only depends on $\lambda$ and $\beta$, and so we can write [5, 6],

$$A(\alpha,\lambda)=\pm 1,\quad B(\beta,\lambda)=\pm 1. \tag{6}$$

By experimental reasons, it is convenient to measure the average of $A$ and $B$ that we denote by $\overline{A}$ and $\overline{B}$ , and then we can write Eq. (6) as

$$\overline{A}(\alpha,\lambda)=\pm 1,\quad \overline{B}(\beta,\lambda)=\pm 1. \tag{7}$$

The events are independent (locality principle) so the correlation is given by the expectation of both events that becomes simply

$$E(\alpha,\beta,\lambda)=E(\alpha,\lambda)E(\beta,\lambda). \tag{8}$$

As $\overline{A}$ and $\overline{B}$ tends to $E(\alpha,\lambda)$ and $E(\beta,\lambda)$, respectively, and integrating to $\lambda$ for eliminating the dependence to hidden variables, we can rewrite the correlation (8) as follows,

$$E(\alpha,\beta)=\int_{\lambda\in\Gamma}\rho(\lambda)\overline{A}(\alpha,\lambda)\overline{B}(\beta,\lambda)d\lambda\ , \tag{9}$$

where $\rho(\lambda)$ is the probability distribution of the hidden variables, $\lambda$, and $\Gamma$ is the space probability. The correlation (9) takes values between $+1$ and $-1$, where $+1$ means the perfect correlation between the polarization of two particles; 0 means that no correlation exists; $-1$ means anticorrelation; and the intermediate values means intermediate correlations.

As we want to know the correlation dependence with the orientation of the polarizer and considering two alternative experimental configurations, $\alpha'$ and $\beta'$, we can write,

$$\begin{aligned}&E(\alpha,\beta)-E(\alpha,\beta')\\&\quad=\int_{\lambda\in\Gamma}\rho(\lambda)[\overline{A}(\alpha,\lambda)\overline{B}(\beta,\lambda)-\overline{A}(\alpha,\lambda)\overline{B}(\beta',\lambda)]d\lambda\\&\quad=\int_{\lambda\in\Gamma}\rho(\lambda)[\overline{A}(\alpha,\lambda)\overline{B}(\beta,\lambda)(1\pm\overline{A}(\alpha',\lambda)\overline{B}(\beta',\lambda)]d\lambda\\&\quad-\int_{\lambda\in\Gamma}\rho(\lambda)[\overline{A}(\alpha,\lambda)\overline{B}(\beta',\lambda)(1\pm\overline{A}(\alpha',\lambda)\overline{B}(\beta,\lambda)]d\lambda.\end{aligned} \tag{10}$$

Using the condition (7) and (9) in Eq. (10), we obtain

$$\begin{aligned}E(\alpha,\beta)-E(\alpha,\beta')&\geq -2-\big(E(\alpha',\beta)+E(\alpha',\beta')\big)\\E(\alpha,\beta)-E(\alpha,\beta')&\leq +2-\big(E(\alpha',\beta)+E(\alpha',\beta')\big)\end{aligned}, \tag{11}$$

which shows that

$$|E(\alpha,\beta)-E(\alpha,\beta')+E(\alpha',\beta)+E(\alpha',\beta')|\leq 2. \tag{12}$$

The term in the left hand of Eq. (12) is known as the Shannon entropy, $S$, and then, we have

$$|S|\leq 2\ , \tag{13}$$

for any LTHV and arbitrary $\alpha$, $\alpha'$, $\beta$, and $\beta'$. Equation (12) is a way to express a Bell inequality, best known as CHSH inequality [4].

The inequality presented in Eq. (12) obeys to all LTHVs, however, the standard interpretation of quantum mechanics do not obey to this inequality as we will see in the following subsection.

### *2.2. Pure Entangled Quantum State*

To demonstrate the violation of the inequality presented in Eq. (12), we consider the state defined by equation Eq. (2).

No matter what is the distance at which both photons are, if we know the polarization of one of them, then we know the polarization of the other, with certain, if the measuring devices of both photons are aligned in the same way.

The probabilities to obtain photons in a given polarization are given by Eq. (5). The correlation of the two-photon states is defined as,

$$\begin{aligned}E(\alpha,\beta)=&P_{V_1',V_2'}(\alpha,\beta)+P_{H_1',H_2'}(\alpha,\beta)\\&-P_{H_1',V_2'}(\alpha,\beta)-P_{V_1',H_2'}(\alpha,\beta).\end{aligned} \tag{14}$$

Replacing Eqs. (5) and (14) in Eq. (12), we obtain the following expression for $S$

$$\begin{aligned}S=&\cos[2(\beta-\alpha)]-\cos[2(\beta'-\alpha)]\\&+\cos[2(\beta-\alpha')]+\cos[2(\beta'-\alpha')].\end{aligned} \tag{15}$$

The parameter $S$ is a function that depends on four variables, $\alpha$, $\beta$, $\alpha'$, and $\beta'$. Then, it is hard to maximize it because it is not possible to separate the variables. A clever way to find the maximum value of $S$ is to find the maximum of each term. In that case, we will obtain $S=4$. However, that goes out of the validation limits of theory. Then, let us determine $\alpha$, $\beta$, $\alpha'$, and $\beta'$ by solving the following linear system,

$$\begin{cases}\beta-\alpha=\pi\\ \beta'-\alpha=\pm\pi/2\\ \beta-\alpha'=\pi\\ \beta'-\alpha'=\pi\end{cases}. \tag{16}$$

Writing Eq. (16) in the matrix form, we have

$$\begin{bmatrix}-1&0&1&0\\-1&0&0&1\\0&-1&1&0\\0&-1&0&1\end{bmatrix}\begin{bmatrix}\alpha\\ \alpha'\\ \beta\\ \beta'\end{bmatrix}=\begin{bmatrix}\pi\\ \pm\pi/2\\ \pi\\ \pi\end{bmatrix} \tag{17}$$

and solving Eq. (17) by Gauss–Jordan method we get

$$\begin{bmatrix}-1&0&1&0\\0&-1&1&0\\0&0&-1&1\\0&0&0&0\end{bmatrix}\begin{bmatrix}\alpha\\ \alpha'\\ \beta\\ \beta'\end{bmatrix}=\begin{bmatrix}\pi\\ \pm\pi/2\\ \pi\\ \mp\pi/2\end{bmatrix}, \tag{18}$$

which is impossible to solve. This means that there are no $\alpha$, $\beta$, $\alpha'$, and $\beta'$ that satisfies the conditions in Eq. (16). However, considering that the maximum value for $S$ leads to $\alpha$, $\beta$, $\alpha'$, and $\beta'$ values that satisfy similar conditions, adding or subtracting a constant $\Delta$ to the above conditions, we obtain the following linear system

$$\begin{cases}\beta-\alpha=\pi\pm\Delta\\ \beta'-\alpha=\pm\pi/2\pm\Delta\\ \beta-\alpha'=\pi\pm\Delta\\ \beta'-\alpha'=\pi\pm\Delta\end{cases}. \tag{19}$$

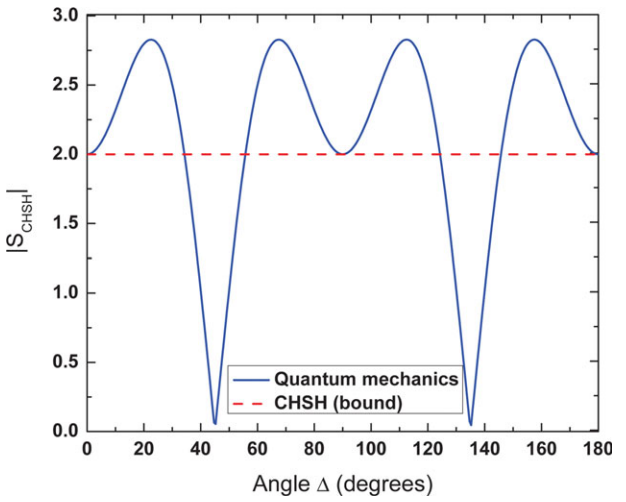


**Figure 2** Shannon entropy $S_{\mathrm{CHSH}}$, as a function of $\Delta$, given by Eq. (22). [Color figure can be viewed in the online issue, which is available at wileyonlinelibrary.com]

Writing Eq. (19) in the matrix form, we get

$$\begin{bmatrix} -1 & 0 & 1 & 0 \\ -1 & 0 & 0 & 1 \\ 0 & -1 & 1 & 0 \\ 0 & -1 & 0 & 1 \end{bmatrix} \begin{bmatrix} \alpha \\ \alpha' \\ \beta \\ \beta' \end{bmatrix} = \begin{bmatrix} \pi \pm \Delta \\ \pm\pi/2 \pm \Delta \\ \pi \pm \Delta \\ \pi \pm \Delta \end{bmatrix}. \tag{20}$$

Solving Eq. (20) by Gauss–Jordan method we get

$$\begin{bmatrix} -1 & 0 & 1 & 0 \\ 0 & -1 & 1 & 0 \\ 0 & 0 & -1 & 1 \\ 0 & 0 & 0 & 0 \end{bmatrix} \begin{bmatrix} \alpha \\ \alpha' \\ \beta \\ \beta' \end{bmatrix} = \begin{bmatrix} \pi \pm \Delta \\ \pi \pm \Delta \\ \pm\pi/2 \pm (2\Delta \vee 0) \\ \mp\pi/2 \pm (4\Delta \vee 2\Delta \vee 0) \end{bmatrix}. \tag{21}$$

The system in Eq. (19)) is just possible when $\Delta = \pm\,\pi/8$ or $\Delta = \pm\,\pi/4$. In Figure 2, we show the Shannon entropy as a function of $\Delta$, and we can see that $|S| > 2$ only when $\Delta = \pm\,\pi/8$, that corresponds to the maximum of $|S|$, whereas for $\Delta = \pm\,\pi/4$, it corresponds to the minimum. This particular system gives the set of solutions,

$$\begin{cases} \alpha \in [0, \pi] \\ \beta = \pi + \Delta + \alpha \\ \alpha' = 2\Delta + \alpha \\ \beta' = \pm\pi/2 - \Delta + \alpha \end{cases}. \tag{22}$$

In case of $\Delta = \pi/8$, we obtain a set of solutions that allow to obtain a value for $S > 2$ which is sufficient for verification of CHSH inequality violation. The parameters $\alpha$, $\beta$, $\alpha'$, and $\beta'$ are called the violation angles. As can be seen from Eq. (22), there are many solutions for the violation angles. The solutions present a maximum value for $S = 2\sqrt{2}$ being those angles called angles of maximum violation. This result was also confirmed numerically.

### *2.3. General Greenberger–Horne–Zeilinger States*

The general GHZ state in which the pure entangled quantum state is included, as described in Eq. (2) can be written for a two photon state as

$$|\Psi\rangle = \cos(\phi)|H\rangle_1|H\rangle_2 + \sin(\phi)|V\rangle_1|V\rangle_2, \tag{23}$$

where $0 < \phi < \pi/2$. These states are important in quantum technologies, namely in quantum cryptography. It is interesting to study these states in Bell's inequalities context. So, let us analyze what states of GHZ family violate the CHSH inequality presented in Eq. (13). To compute the Shannon entropy we need to compute first the correlation function by a state given by Eq. (23). The correlation function can be calculated in the similar way as in previous sections, and it has the following expression,

$$E(\alpha, \beta) = \cos(2\alpha)\cos(2\beta) + \sin(2\phi)\sin(2\alpha)\sin(2\beta). \tag{24}$$

So, the Shannon entropy becomes

$$\begin{aligned} S = \frac{1}{2}\Big\{ & \big(1 - \sin(2\phi)\big)\big[\cos(2(\alpha+\beta)) - \cos(2(\alpha+\beta')) \\ & + \cos(2(\alpha'+\beta)) + \cos(2(\alpha'+\beta'))\big] \\ & + \big(1 + \sin(2\phi)\big)\big[\cos(2(\alpha-\beta)) - \cos(2(\alpha-\beta')) \\ & + \cos(2(\alpha'-\beta)) + \cos(2(\alpha'-\beta'))\big]\Big\}. \end{aligned} \tag{25}$$

As we can see in Section 2.2, the maximum of $S$ is so defined that instead of four independent variables, $\alpha$, $\alpha'$, $\beta$, and $\beta'$, there is only one, $\Delta$. Thus, we can assume that $\alpha$ and $\alpha'$ are constant and their values are the same as that in the case $\phi = \pm\,\pi/4$ and only $\beta$ and $\beta'$ depend on $\phi$, so the Shannon entropy becomes

$$S = \cos(2\beta) - \cos(2\beta') + \sin(2\phi)\big(\sin(2\beta) + \sin(2\beta')\big). \tag{26}$$

To determine the maximum of $S$, we calculate the zero of the $S$ gradient ($\nabla_{\beta,\beta'} S = 0$). One of the solutions of $\nabla_{\beta,\beta'} S = 0$ is $\cos(2\beta) = -\cos(2\beta')$. When we replace this solution in Eq. (26), we obtain $S$ dependent only of $\beta(\beta')$, thus, we obtain the result

$$\cos(2\zeta) = \pm\frac{1}{\sqrt{1 + \sin^2(2\phi)}}, \tag{27}$$

with $\zeta = \beta, \beta'$, for which, $S$ is maximum. Taking into account that $\cos(2\beta) = -\cos(2\beta')$ and replacing Eq. (27) in Eq. (26), we obtain the following form by the maximum of the Shannon entropy,

$$S = 2\sqrt{\sin^2(2\phi) + 1}. \tag{28}$$

Being the maximum of the Shannon entropy a sufficient condition for the verification of the violation of CHSH inequality, the expression given by Eq. (28) and illustrated in Figure 3 gives us the solution for the violation of CHSH inequality by all states of the GHZ states family. We can see that the maximum of violation happens for $\phi = \pi/4$, which corresponds to the pure entangled quantum state and that we will use in Section 3, for the experimental verification of the violation of CHSH inequality.

### *2.4. General States*

In this section, we will calculate the solution for the violation of CHSH inequality for any arbitrary state of two particles. The method developed by Horodeckis family [17] allows to verify if an arbitrary state violates or not CHSHs inequality. However, we will find the solution for the maximum of Shannon entropy for any state of two particles, analyzing the correlation function, like in previous section.

A general state of two particles has the following form,

$$|\Psi\rangle = a|H\rangle_1|H\rangle_2 + b|H\rangle_1|V\rangle_2 + c|V\rangle_1|H\rangle_2 + d|V\rangle_1|V\rangle_2, \tag{29}$$

where $\sqrt{|a|^2 + |b|^2 + |c|^2 + |d|^2} = 1$. To calculate the Shannon entropy, we need to calculate first the correlation function that has the following expression

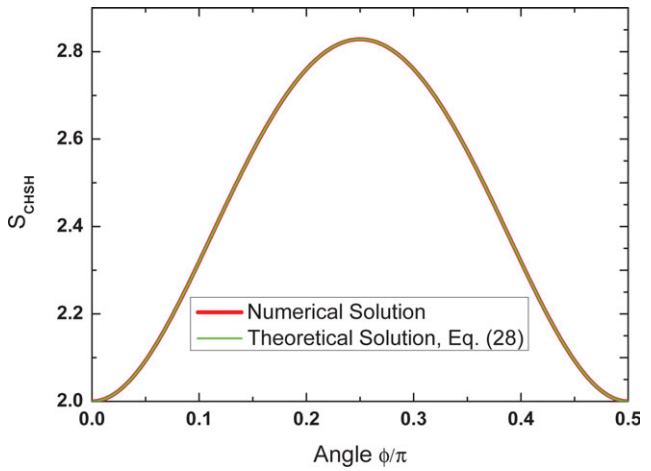


**Figure 3** Maximum of Shannon entropy by general GHZ states as a function of $\phi$. [Color figure can be viewed in the online issue, which is available at wileyonlinelibrary.com]

$$\begin{aligned} E(\alpha,\beta) = {} & (|a|^2 - |b|^2 - |c|^2 + |d|^2)\cos(2\alpha)\cos(2\beta) \\ & + (a^\dagger b + ab^\dagger - c^\dagger d - cd^\dagger)\cos(2\alpha)\sin(2\beta) \\ & + (a^\dagger c + ac^\dagger - b^\dagger d - bd^\dagger)\sin(2\alpha)\cos(2\beta) \\ & + (a^\dagger d + ad^\dagger + b^\dagger c + bc^\dagger)\sin(2\alpha)\sin(2\beta). \end{aligned} \tag{30}$$

So, the Shannon entropy becomes,

$$\begin{aligned} S = {} & (|a|^2 - |b|^2 - |c|^2 + |d|^2)\{\cos(2\alpha)[\cos(2\beta) - \cos(\beta')] \\ & + \cos(2\alpha')[\cos(2\beta) + \cos(2\beta')]\} \\ & + (a^\dagger b + ab^\dagger - c^\dagger d - cd^\dagger)\{\cos(2\alpha)[\sin(2\beta) - \sin(\beta')] \\ & + \cos(2\alpha')[\sin(2\beta) + \sin(2\beta')]\} \\ & + (a^\dagger c + ac^\dagger - b^\dagger d - bd^\dagger)\{\sin(2\alpha)[\cos(2\beta) - \cos(\beta')] \\ & + \sin(2\alpha')[\cos(2\beta) + \cos(2\beta')]\} \\ & + (a^\dagger d + ad^\dagger + b^\dagger c + bc^\dagger)\{\sin(2\alpha)[\sin(2\beta) - \sin(\beta')] \\ & + \sin(2\alpha')[\sin(2\beta) + \sin(2\beta')]\}. \end{aligned} \tag{31}$$

We can rewrite Eq. (31) in following way,

$$\begin{aligned} S = {} & A_1\mathfrak{S}_1(\alpha,\beta,\alpha',\beta') + A_2\mathfrak{S}_2(\alpha,\beta,\alpha',\beta') \\ & + A_3\mathfrak{S}_3(\alpha,\beta,\alpha',\beta') + A_4\mathfrak{S}_4(\alpha,\beta,\alpha',\beta'), \end{aligned} \tag{32}$$

where

$$\begin{aligned} A_1 &= (|a|^2 - |b|^2 - |c|^2 + |d|^2) \\ A_2 &= (a^\dagger b + ab^\dagger - c^\dagger d - cd^\dagger) \\ A_3 &= (a^\dagger c + ac^\dagger - b^\dagger d - bd^\dagger) \\ A_4 &= (a^\dagger d + ad^\dagger + b^\dagger c + bc^\dagger). \end{aligned} \tag{33}$$

The functions $\mathfrak{S}_j$ for $j = 1\ldots4$ are trigonometric functions, and by the properties of trigonometric functions and taking into account the definition of $S$, the maximum of $S$ is equal to

$$\max(S) = 2\sqrt{A_1^2 + A_2^2 + A_3^2 + A_4^2}. \tag{34}$$

The factor 2 before the square root, arises from the maximum of the $\mathfrak{S}_j$ function, $\max(\mathfrak{S}_j) = 2$. Note that $A_j$ is the same as in the correlation function given by Eq. (30). The solution (34) gives us the maximum of $S$. In Figure 4, we can see the maximum of $S$ for different configuration of parameters $a$, $b$, $c$, and $d$. In Figure 4, the parameters $a$, $b$, $c$, and $d$ are always real, with $(a,b,c,d) \in \mathbb{R}^4$, and we replace them for the coordinates of the hyper-sphere with dimension 4, that is,

$$\begin{aligned} a &= \cos(\phi_1) \\ b &= \sin(\phi_1)\cos(\phi_2) \\ c &= \sin(\phi_1)\sin(\phi_2)\cos(\phi_3) \\ d &= \sin(\phi_1)\sin(\phi_2)\sin(\phi_3). \end{aligned} \tag{35}$$

The solution given by Eqs. (33–35) coincides with the solution obtained numerically.

The maximum of the Shannon entropy for an arbitrary state of two particles only depends on the definition of the correlation function. This is an unexpected result, but understandable, as it is the correlation function that reflects the correlation between the particles. The generalization of this result for $N$ particles can be thus achieved in a simple way.

### *2.5. Nonentangled Quantum States*

In this subsection, we will verify that the violation of Bell's inequality is a characteristic of entangled states only. Of course that the nonentangled states are included in previous subsection, but in this subsection, we will study them in the explicit way, to show that they do not have "nonlocal" properties. In nonentangled quantum states, the events are independent, so $E(\alpha,\beta) =$

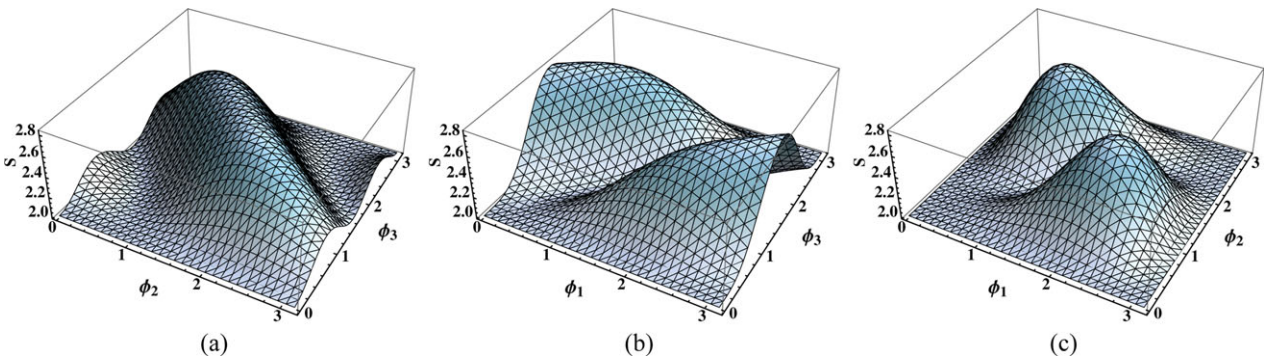


**Figure 4** Profiles of the maximum of $S$ for a general state with parameters given in (35). (a) Shannon entropy as a function of $\phi_2$ and $\phi_3$ for $\phi_1 = \pi/4$; (b) Shannon entropy as a function of $\phi_1$ and $\phi_3$ for $\phi_2 = \pi/4$; (c) Shannon entropy as a function of $\phi_1$ and $\phi_2$ for $\phi_3 = \pi/4$. [Color figure can be viewed in the online issue, which is available at wileyonlinelibrary.com]

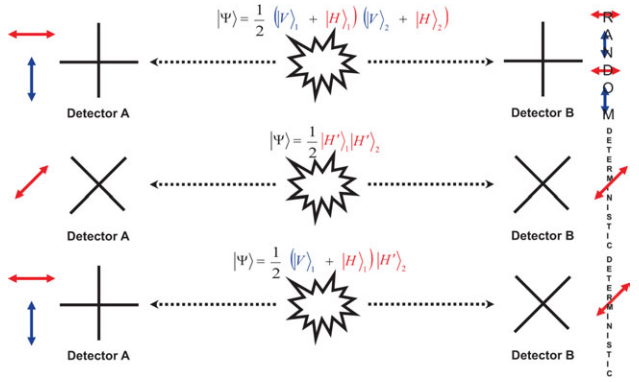


**Figure 5** Scheme of polarization measurement using two different basis. The state is written as a function of the basis of the measurement device. [Color figure can be viewed in the online issue, which is available at wileyonlinelibrary.com]

$E(\alpha)E(\beta)$. Using this property, we obtain the Shannon entropy as in Eq. (12),

$$\begin{aligned} S &= E(\alpha)E(\beta) - E(\alpha)E(\beta') + E(\alpha')E(\beta) + E(\alpha')E(\beta') \\ S &= E(\alpha)\big(E(\beta) - E(\beta')\big) + E(\alpha')\big(E(\beta) + E(\beta')\big) \end{aligned} \quad . \tag{36}$$

$S$ is a function of $\alpha$, $\beta$, $\alpha'$, and $\beta'$ with the separate variables. The maximum of $S$ is the maximum of each function. The maximum of $E(\alpha) = E(\alpha') = 1$, so $S$ reduces to $2E(\beta)$, in which the maximum is 2, and then, we conclude that the result is in agreement with CHSH inequality presented in Eq. (12).

In this section, we consider, without loss of generality, a system with two photons in following state,

$$|\psi\rangle = \frac{1}{2}\Big[(|H\rangle + |V\rangle)_1 \otimes (|H\rangle + |V\rangle)_2\Big], \tag{37}$$

which can be written as,

$$|\psi\rangle = \frac{1}{2}\Big[|H\rangle_1|H\rangle_2 + |H\rangle_1|V\rangle_2 + |V\rangle_1|H\rangle_2 + |V\rangle_1|V\rangle_2\Big]. \tag{38}$$

This state can be split up into individual states for the two photons that are also nonentangled. Such as in the previous section, we consider two particles that travel in opposite directions and that will be detected by devices that measure their polarization and that are rotated by $\alpha$ for particle 1 and by $\beta$ for particle 2, in relation to the horizontal state. The state of the measurement device rotated by $\alpha$ is according to Eqs. (3) and (4).

Similarly, to entangled states, we consider that the measurement devices are not aligned with the polarization of photons. The probabilities of having photons in a given polarization state are then,

$$\begin{aligned} P_{V_1,V_2}(\alpha,\beta) &= |\langle V|_\alpha \langle V|_\beta|\psi\rangle|^2 = \frac{1}{4}|\cos(\beta-\alpha) - \sin(\beta+\alpha)|^2; \\ P_{H_1,V_2}(\alpha,\beta) &= |\langle H|_\alpha \langle V|_\beta|\psi\rangle|^2 = \frac{1}{4}|\cos(\beta+\alpha) - \sin(\beta-\alpha)|^2; \\ P_{V_1,H_2}(\alpha,\beta) &= |\langle V|_\alpha \langle H|_\beta|\psi\rangle|^2 = \frac{1}{4}|\cos(\beta+\alpha) + \sin(\beta-\alpha)|^2; \\ P_{H_1,H_2}(\alpha,\beta) &= |\langle H|_\alpha \langle H|_\beta|\psi\rangle|^2 = \frac{1}{4}|\cos(\beta-\alpha) + \sin(\beta+\alpha)|^2. \end{aligned} \tag{39}$$

We can see by Figure 5 and by the probabilities given in Eq. (39) that only when $\beta - \alpha = 0$ and $\beta + \alpha = 0$ or when $\beta - \alpha = \pi/2$ and $\beta + \alpha = \pi/2$, we have the situation of perfectly randomness. All the cases are in the intermediate situation, except when the angle of the polarizer is 45°. In this case, the measurement is deterministic because it reduces to a well-defined state, coincident with the transmission direction of the polarizer.

Using the example of the state (38) we can calculate the Shannon entropy. For that we replace Eqs. (39) and (8) in Eq. (12), and we obtain the following expression for $S$,

$$\begin{aligned} S = \sin(2\alpha)[\sin(2\beta) - \sin(2\beta')] \\ + \sin(2\alpha')[\sin(2\beta) + \sin(2\beta')]. \end{aligned} \tag{40}$$

In this case, the parameter $S$ is a function with separate variables, achieving the maximum value when all terms are maximum. When $\alpha = \alpha' = \pi/2$, $S = 2\sin(2\beta)$ (independent of $\beta'$), and the maximum value that it can assume is $S = 2$, that is, it is in agreement with Bell theory and the LTHVs.

### 3. EXPERIMENTAL VERIFICATION

To generate polarization-entangled photon pairs, we used the experimental setup presented in Figure 6. A pump from a tunable laser source, centered at 1550.918 nm, [close to the zero-dispersion wavelength of the HNLF used], with a full width at half maximum of 830 ps, was modulated at a repetition rate of 2.2 MHz. After amplification by an erbium-doped fiber amplifier and filtering, photons are aligned at 45° and launched into a Sagnac fiber loop, which consists in a four-port polarization beam splitter (PBS), an HNLF with a length equal to 150 m, a nonlinear coefficient, $\gamma \approx 10.5\ \mathrm{W}^{-1}\ \mathrm{km}^{-1}$, and the zero-dispersion wavelength at around 1550 nm, and two polarization controllers (PCs), PC3 and PC4. The power at the input of each arm of the HNLF was 2.2 mW. The PBS divides the pump pulses into horizontal ($|H\rangle$) and vertical ($|V\rangle$) polarization components, having each one equal optical power. The two components generate signal-idler photon pairs $|H\rangle_s|H\rangle_i$ and $|V\rangle_s|V\rangle_i$, while propagating in the loop in the counterclockwise and clockwise directions, respectively. The PCs (PC3 and PC4) were adjusted so that the generated photon pairs were properly output from the loop, at port-4. The polarization-entangled photon pairs result in the superposition state given by,

$$|\psi_{\text{entangled}}\rangle = \frac{1}{\sqrt{2}}\Big[|H\rangle_s|H\rangle_i + |V\rangle_s|V\rangle_i\Big]. \tag{41}$$

At the loop output, the pump photons are suppressed and the idler and signal photons go into an arrayed waveguide grating (AWG), which sends signal photons on one path, and idler photons to the other. AWG output channels with peak wavelengths of $\lambda_s = 1547.715$ nm and $\lambda_i = 1554.134$ nm were used for the signal and idler, respectively. Next, fixed optical filters centered at the AWGs output wavelength channels are used in each arm to assure that only signal ($F_s$) or idler ($F_i$) photons pass, and all the other wavelengths are suppressed. The pump, signal, and idler photons, with frequencies $\omega_p$, $\omega_s$, and $\omega_i$, respectively, satisfies the phase-matching condition, $2\omega_p = \omega_s + \omega_i$ [22].

The states of polarization of the signal and idler photons were adjusted using a quarter waveplate and an half waveplate, so that the two photons experienced the same polarization change after they were separated by the AWG. Each photon was lead into a rotatable linear polarizer (RLP1 and RLP2) and was detected with an InGaAs/InP avalanche photodiode (APD1 and APD2) from IdQuantique, operating in a gated Geiger mode [23]. APD1 (id201) has a dark count probability per time gate,

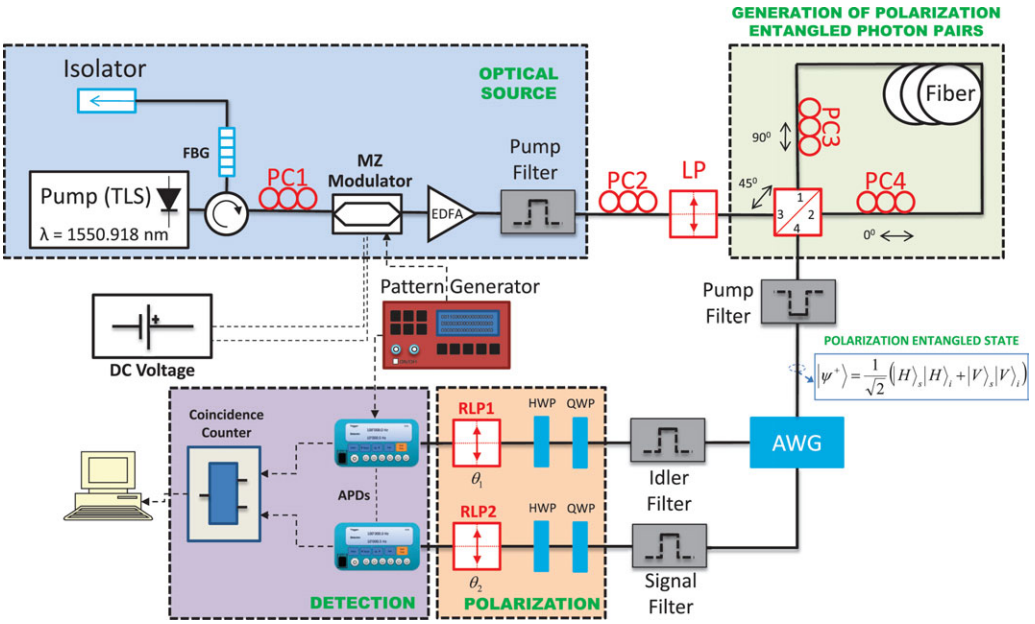


**Figure 6** Schematics of the experimental setup used for polarization-entangled photon pair generation through spontaneous FWM and coincidence detection. [Color figure can be viewed in the online issue, which is available at wileyonlinelibrary.com]

$t_g = 2.5$ ns, of $P_{dc} < 5 \times 10^{-6}$ ns$^{-1}$, and a quantum detection efficiency, $\eta_D \sim 10\%$ [24]. APD2 (id200) has a dark count probability per time gate, $t_g = 2.5$ ns, of $P_{dc} < 5 \times 10^{-5}$ ns$^{-1}$, and a quantum detection efficiency, $\eta_D \sim 10\%$ [25]. To avoid afterpulses, a 10 $\mu$s deadtime was applied to both detectors. The electric signals from the APDs were input into a time tagging module (TTM) for coincidence measurements. The TTM worked in a continuous mode, with a time resolution of 82.3 ps.

For experimental demonstration of polarization entanglement of the generated photon pairs, we measured the coincidence rate for 16 combinations of polarizer settings ($\theta_1 = -45°$, 0°, 45°, 90°; $\theta_2 = -22.5°$, 22.5°, 67.5°, 112.5°) to obtain the $S$ value of the CHSH inequality [4].

In Figure 7, we present coincidence and single counts detected over 60 s, varying the RLP2 ($\theta_2$), whereas the RLP1 ($\theta_1$) is fixed for values 0°, 45°, and 90°, −45°. In Figure 7(a), we present signal single counts, and in Figure 7(b) are presented idler single counts, just as an example, as the other results obtained experimentally present similar behavior. The fact that single counts are roughly constant means that single photons are unpolarized or randomly polarized [18].

In Table 1, we present the single and coincidence counts as a function of polarizer angles, $\theta_1$ and $\theta_2$ obtained experimentally.

Using the experimental data obtained we calculated the parameters defined in Eqs. (14) and (15). The uncertainty of the quantity $S$ can be also calculated, and is given by,

$$\sigma_S = \sqrt{\sum_{i=1}^{16} C_i \left(\frac{\partial S}{\partial C_i}\right)^2}, \tag{42}$$

where the uncertainty of the $i$th measurement, $C_i$, is $\sigma_{C_i} = \sqrt{C_i}$ [26].

The correlation coefficients required for the CHSH inequality and the respective uncertainties are presented in Table 2.

From the measured values, we obtained a parameter $S = 2.47 \pm 0.17$, when accidental coincidences were subtracted, which indicates that we produced entangled photon pairs with

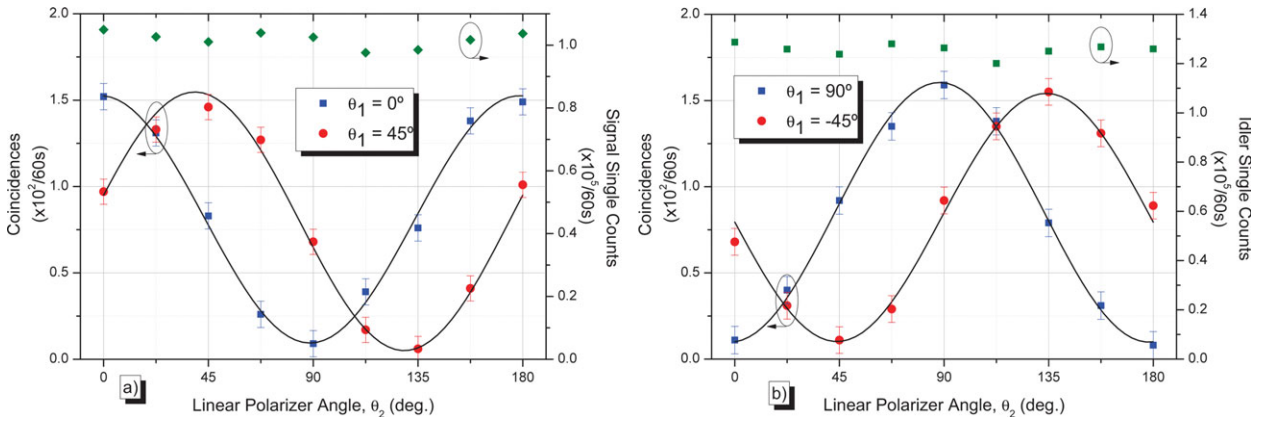


**Figure 7** Coincident and single counts as a function of $\theta_2$, while a) $\theta_1 = 0°$, 45°, and b) $\theta_1 = 90°$, −45° were kept fixed. The solid curve is a sinusoidal fit to the experimental data. Error bars are a 5% deviation in relation to the maximum value, in each case. [Color figure can be viewed in the online issue, which is available at wileyonlinelibrary.com]

**TABLE 1 Single ($N_{\theta_1}$, $N_{\theta_2}$) and Coincidence ($C$) Counts as a Function of Polarizer Angles ($\theta_1$, $\theta_2$)**

| $\theta_1$ | $\theta_2$ | $N_{\theta_1}$ | $N_{\theta_2}$ | $C$ |
|---|---|---|---|---|
| 0° | 22.5° | 102,660 | 122,880 | 131 |
| 90° | 112.5° | 102,660 | 120,060 | 138 |
| 0° | 112.5° | 97,620 | 129,000 | 39 |
| 90° | 22.5° | 105,360 | 125,880 | 40 |
| 0° | 67.5° | 103,920 | 123,420 | 26 |
| 90° | 157.5° | 98,880 | 126,780 | 31 |
| 0° | 157.5° | 101,700 | 121,500 | 138 |
| 90° | 67.5° | 97,980 | 127,980 | 135 |
| 45° | 22.5° | 102,840 | 125,280 | 133 |
| −45° | 112.5° | 105,840 | 119,220 | 135 |
| 45° | 112.5° | 103,260 | 123,480 | 17 |
| −45° | 22.5° | 102,720 | 116,040 | 31 |
| 45° | 67.5° | 101,340 | 119,940 | 127 |
| −45° | 157.5° | 101,880 | 124,740 | 131 |
| 45° | 157.5° | 102,660 | 117,240 | 41 |
| −45° | 67.5° | 99,300 | 123,780 | 29 |

**TABLE 2 Measured Correlation Coefficients Required for the CHSH Inequality**

| $E(\theta_1,\theta_2)$ | (0°, 22.5°) | (0°, 67.5°) | (45°, 22.5°) | (45°, 67.5°) |
|---|---|---|---|---|
| Value | 0.5460 | −0.6545 | 0.6962 | 0.5732 |
| Error | 0.0396 | 0.0445 | 0.0469 | 0.0418 |

strong correlation, and thus, we observed the violation of CHSH inequality by 2.7 standard deviations. Coincidence counts present fringe visibilities higher than 86%. This result is consistent with quantum mechanics, as we presented in previous sections.

## 4. CONCLUSIONS

We discussed Bell's inequality and demonstrated theoretically that the maximum violation of CHSH inequality, a special case of Bell's inequality, is observed for $S = 2\sqrt{2}$, for the pure entangled quantum state.

We generalized the discussion for general GHZ states and also for an arbitrary state of two particles. Thus, we found the solution that allows us to check if a given state violates or not CHSH's inequality, or in other words, if a given state can or not be describe by a LTHV. Using a nonentangled quantum state, we also showed theoretically that the violation of CHSH inequality is a characteristic of entangled quantum states only.

We also implemented an experimental setup suitable for verification of the violation of CHSH inequality. Polarization-entangled photon pairs were obtained using the spontaneous FWM process in a fiber loop. With accidental coincidences subtracted, we obtained a visibility for the coincidence fringes of more than 86%, and thus observed the violation of CHSH inequality by 2.7 standard deviations, confirming the generation of entangled-photon pairs.

## ACKNOWLEDGMENTS

This work was partially supported by the Fundação para a Ciência e Tecnologia, FCT, through the Laboratório Associado (IT/LA) program, projects ''P-Quantum - Pratical Quantum Communications'' and ''QuantPrivTel - Quantum Private Telecommunications'' project (PTDC/EEA-TEL/103402/2008), FEDER and PTDC programs, and the PhD Grant SFRH/BD/79482/2011, from FCT.

## REFERENCES

1. C.H. Bennett and G. Brassard, Quantum cryptography: Public key distribution and coin tossing, Bangalore, India, 1984, pp. 175–179.
2. A.K. Ekerk, Quantum cryptography based on Bell's theorem, Rev Lett 67 (1991), 661–663.
3. V. Scarani and N. Gisin, Quantum communication between *N* partners and Bell's inequalities, Phys Rev Lett 87 (2001), 117901.
4. J.F. Clauser, M.A. Horne, A. Shimony, and R.A. Holt, Proposed experiment to test local hidden-variable theories, Phys Rev Lett 23 (1969), 880–884.
5. J.S. Bell, On the problem of hidden variables in quantum mechanics, Rev Mod Phys 38 (1966), 447–452.
6. J.S. Bell, The theory of local beables, 2 ed., Cambridge University Press, London, England, 2004.
7. S.J. Freedman and J.F. Clauser, Experimental test of local hidden-variable theories, Phys Rev Lett 28 (1972), 938–941.
8. A. Aspect, P. Grangier, and G. Roger, Experimental tests of realistic local theories via Bell's theorem, Phys Rev Lett 47 (1981), 460–463.
9. G. Weihs, T. Jennewein, C. Simon, H. Weinfurter, and A. Zeilinger, Violation of Bell's inequality under strict Einstein locality conditions, Phys Rev Lett 81 (1998), 5039–5043.
10. A. Aspect, P. Grangier, and G. Roger, Experimental realization of Einstein-Podolsky-Rosen-Bohm Gedankenexperiment: A New violation of Bell's inequalities, Phys Rev Lett 49 (1982), 91–94.
11. L.J. Wang, C.K. Hong, and S.R. Friberg, Generation of correlated photons via four-wave mixing in optical fibres, J Opt B: Quant Semiclassical Opt 3 (2001), 346–352.
12. V. Capasso, D. Fortunato, and F. Selleri, Sensitive observables of quantum mechanics, Int J Theoret Phys 7 (1973), 319–326.
13. N. and Gisin, Bell's inequality holds for all non-product states, Phys Lett A 154 (1991), 201–202.
14. N. Gisin and A. Peres, Maximal violation of Bell's inequality for arbitrarily large spin, Phys Lett A 162 (1992), 15–17.
15. S. Popescu and D. Rohrlich, Generic quantum nonlocality, Phys Lett A 166 (1992), 293–297.
16. S. Popescu, Bell's inequalities versus teleportation: What is nonlocality?, Phys Rev Lett 72 (1994), 797–799.
17. R. Horodecki, P. Horodecki, and M. Horodecki, Violation Bell inequality by mixed spin-1/2 states: Necessary and sufficient condition, Phys Lett A 200 (1995), 340–344.
18. X. Li, P.L. Voss, J.E. Sharping, and P. Kumar, Optical-Fiber source of polarization-entangled photons in the 1550 nm telecom band, Phys Rev Lett 94 (2005), 053601.
19. G. Agrawal, Nonlinear fiber optics, 4th ed. Academic Press, Orlando, FL, 2007.
20. H. Takesue and K. Inoue, Generation of 1.5-μm band time-bin entanglement using spontaneous fiber four-wave mixing and planar light-wave circuit interferometers, Phys Rev A 72 (2005), 041804.
21. N.A. Silva, N.J. Muga, and A.N. Pinto, Effective nonlinear parameter measurement using FWM in optical fibers in a low power regime, IEEE J Quant Electron 46 (2010), 285–291.
22. H. Takesue and K. Inoue, Generation of polarization-entangled photon pairs and violation of Bell's inequality using spontaneous four-wave mixing in a fiber loop, PRA 70 (2004), 031802.
23. G. Ribordy, N. Gisin, O. Guinnard, D. Stucki, M. Wegmuller, and H. Zbinden, Photon counting at telecom wavelengths with commercial InGaAs/InP avalanche photodiodes: current performance, J Modern Opt 51 (2004), 1381–1398.
24. idQuantique, id 201 Single-Photon Detector Module – Operating Guide, Version 4.0, 2008.
25. idQuantique, id 200 Single-Photon Detector Module – Operating Guide, Version 2.2, 2005.
26. D. Dehlinger and M.W. Mitchell, Entangled photons, nonlocality, and Bell inequalities in the undergraduate laboratory, Am J Phys 70 (2002), 903–910.